Floquet solutions in a parity-time-symmetric Rabi model

M. Baradaran, Daniel Braak, L. M. Nieto, S. Zarrinkamar

Angaben zur Veröffentlichung / Publication details:

Baradaran, M., Daniel Braak, L. M. Nieto, and S. Zarrinkamar. 2026. “Floquet solutions in a parity-time-symmetric Rabi model.” *Physical Review Research* 8 (1): 013097. https://doi.org/10.1103/2h1h-svtx.

Floquet solutions in a parity-time-symmetric Rabi model

M. Baradaran [1,*] D. Braak [2,†] L. M. Nieto [3,‡] and S. Zarrinkamar [3,4,§]

[1]*Department of Physics, Faculty of Science, University of Hradec Králové, Rokitanského 62, 500 03 Hradec Králové, Czechia*

[2] *Institute of Physics, University of Augsburg, 86135 Augsburg, Germany*

[3]*Departamento de Física Teórica, Atómica y Óptica, Laboratory for Disruptive Interdisciplinary Science (LaDIS), Universidad de Valladolid, 47011 Valladolid, Spain*

[4]*Departament of Basic Sciences, Garmsar Branch, Islamic Azad University, Garmsar, Iran*

(Received 25 February 2025; accepted 10 January 2026; published 28 January 2026)

It is shown that a semiclassical Rabi model with parity-time ($\mathcal{PT}$) symmetry possesses quasiexact solutions, which can be found using the Lie-algebraic approach. These solutions are located precisely at the exceptional points of the spectrum, the boundaries of the $\mathcal{PT}$-symmetric phase. The corresponding constraints on the model parameters can be interpreted as a resonance relationship between the constant and periodic driving terms. For sufficiently large resonance ratio and judiciously chosen parameters, we find that the time evolution of the complete qubit can be described exactly.

DOI: 10.1103/2h1h-svtx

I. INTRODUCTION

The concept of parity-time ($\mathcal{PT}$) symmetry [1,2] and its experimental verification in optics [3,4] has motivated a wide range of research on this topic. In recent years, experimental evidence for parity-time symmetries has been found in diverse fields, such as microresonators [5], microcavities [6], quantum critical phenomena [7], quantum circuits [8], quantum walks [9], photonic crystals [10], sensor telemetry [11], wireless power transfer [12], integrated electronics [13] and photonics [14], and photonic topological insulators [15].

On the other hand, the Rabi model [16], which successfully explains the simplest manifestation of light-matter interaction by coupling a two-level system to a single radiation mode, has been the subject of recent research due to its applications in various physical and interdisciplinary fields, including quantum optics, communication technology, quantum information technology, laser physics, and solid-state physics [17]. Numerous current investigations combine the Rabi model with $\mathcal{PT}$ symmetry from both theoretical and experimental perspectives.

In Ref. [17], a non-Hermitian semiclassical Rabi model with an imaginary periodic driving term was studied in the Floquet picture and shown to exhibit (broken) $\mathcal{PT}$ symmetry. The authors applied a perturbative approach beyond the rotating-wave approximation and showed that the non-Hermitian analog of the Bloch-Siegert shift appears in the case of maximum $\mathcal{PT}$ symmetry breaking. Experimental implementations of these models include spatially modulated loss waveguides (see, for example, Ref. [18]). The stabilization of a non-Hermitian Rabi Hamiltonian by a periodic driving field and its correspondence to the band structure of a particular lattice Hamiltonian via the Floquet operator is addressed in Ref. [19].

In a very recent experimental survey, $\mathcal{PT}$ symmetry-breaking transitions are reported using single ultracold atoms [20]. Anisotropic and asymmetric generalizations of the quantum Rabi model, with periodic driving, have been analyzed in the Floquet picture [21]. A generalized adiabatic approximation has been applied to the $\mathcal{PT}$-symmetric quantum Rabi model, and the so-called exceptional points (EPs) are discussed in depth in relation to their Hermitian analog, the Juddian level crossings [22]. On the other hand, multiphoton resonances, where simultaneous production of several photons can occur by downconversion of a high-frequency pump, are of great importance in the study of phase-space crystals [23], quantum error correction [24], and superconducting cavities, where notable features are observed, including the higher order squeezing [25].

In a related study, Xie *et al.* [26] investigated the effect of a periodic modulation on the $\mathcal{PT}$ symmetry of a non-Hermitian Rabi model with periodic excitation and balanced gain and loss terms. They showed that, under the multiple-photon resonance conditions, the model admits exact Floquet solutions for certain special parameter ratios. In this work, we revisit the model by exploring its hidden algebraic structure within the framework of quasiexact solvability, and further extend the results through detailed numerical investigations. Especially, we note the existence of two linearly independent exact Floquet solutions for (almost) the same parameter set. The paper is organized as follows: first, we review the model studied in Ref. [26]. Then, we show that, through appropriate transformations, the resulting ordinary differential equation can be written in terms of $sl(2)$ generators in a finite-dimensional

*Contact author: marzieh.baradaran@uhk.cz
†Contact author: daniel.braak@uni-a.de
‡Contact author: luismiguel.nieto.calzada@uva.es
§Contact author: saber.zarrinkamar@uva.es

representation if certain constraints on the parameters are satisfied [27]; these are then interpreted as resonance conditions. Next, we present the numerical results and analysis of the n photon constraints, the Floquet quasienergy spectrum, and the time evolution of the "nearly degenerate" Floquet states mentioned above. The conclusions are presented in the last section. Supplementary numerical data and analysis are included in Appendixes A and B.

II. FORMULATION AND GENERAL SOLUTION VIA LIE-ALGEBRAIC APPROACH

We consider the following non-Hermitian time-dependent Hamiltonian [26]:

$$H = i\frac{\gamma}{2}\sigma_z + \frac{\nu(t)}{2}\sigma_x, \tag{1}$$

where $\sigma_{x,z}$ are Pauli matrices acting on a pseudospinor $\Psi(t)^{\mathsf{T}} = (a_1(t), a_2(t))^{\mathsf{T}}$ and $\nu(t) = \nu_0 + \nu_1\cos(\omega t)$, being ν_1 and ω the modulation amplitude and frequency, respectively, while ν_0 represents the qubit splitting energy. In addition, γ denotes the strength of the loss/gain term, characteristic of $\mathcal{PT}$-symmetric dissipative systems. Hence, the two-level probability amplitudes $a_1(t)$ and $a_2(t)$ satisfy the coupled first-order differential equations:

$$\begin{aligned} i\frac{da_1(\tau)}{d\tau} &= \frac{\nu(\tau)}{2\omega}a_2(\tau) + i\frac{\gamma}{2\omega}a_1(\tau), \\ i\frac{da_2(\tau)}{d\tau} &= \frac{\nu(\tau)}{2\omega}a_1(\tau) - i\frac{\gamma}{2\omega}a_2(\tau), \end{aligned} \tag{2}$$

coming from the Schrödinger equation $H\Psi(t) = i\partial_t\Psi(t)$, where we have set $\tau = \omega t$ and $\hbar = 1$. Following Ref. [26], we introduce the combinations

$$c_1(\tau) = (a_1(\tau) + a_2(\tau))/2, \quad c_2(\tau) = (a_1(\tau) - a_2(\tau))/2, \tag{3}$$

which yield after decoupling the second-order ODEs [26],

$$\begin{aligned} \frac{d^2c_1(\tau)}{d\tau^2} + \left(\frac{\nu^2(\tau)}{4\omega^2} + \frac{i}{2\omega}\frac{d\nu(\tau)}{d\tau} - \frac{\gamma^2}{4\omega^2}\right)c_1(\tau) = 0, \\ \frac{d^2c_2(\tau)}{d\tau^2} + \left(\frac{\nu^2(\tau)}{4\omega^2} - \frac{i}{2\omega}\frac{d\nu(\tau)}{d\tau} - \frac{\gamma^2}{4\omega^2}\right)c_2(\tau) = 0. \end{aligned} \tag{4}$$

Formally, these decoupled equations resemble one-dimensional, time-independent Schrödinger equations where the position coordinate is replaced by the time t, the energy eigenvalue is negative $(-\gamma^2/4)$, and the potentials $-\nu^2(t)/4 \mp i\dot{\nu}(t)/2$ are bounded but not real: They become $\mathcal{PT}$ symmetric if $\nu(t)$ is even in t, as in our case.

Let us now define the complex variable $z(\tau)$ and the functions $\phi_j(z)$:

$$z = e^{i\tau} \quad \text{and} \quad c_j(z) = e^{\frac{\nu_1}{2\omega}\cos(\tau)}z^{-\frac{\nu_0}{2\omega}}\phi_j(z), \quad j = 1, 2. \tag{5}$$

After eliminating $\phi_2(z)$, we obtain the following second-order differential equation for $\phi_1(z) \equiv \phi(z)$ [26]:

$$\begin{aligned} z^2\frac{d^2\phi(z)}{dz^2} + \left(\frac{\nu_1}{2\omega}z^2 + \left(1 - \frac{\nu_0}{\omega}\right)z - \frac{\nu_1}{2\omega}\right)\frac{d\phi(z)}{dz} \\ + \left(\frac{\gamma^2 - \nu_1^2}{4\omega^2} + \frac{\nu_1}{2\omega}\left(1 - \frac{\nu_0}{\omega}\right)z\right)\phi(z) = 0. \end{aligned} \tag{6}$$

This equation has the form of an eigenvalue equation $\tilde{H}\phi(z) = \lambda\phi(z)$ with fixed eigenvalue $\lambda = 0$. We will now show that the differential operator $\tilde{H}$ on Eq. (6) has a hidden algebraic structure if certain conditions are met, which will be specified later. This means that $\tilde{H}$ can be expressed as an element of the universal enveloping algebra of $sl(2)$, acting on a finite-dimensional representation. The general form of such a quasiexactly solvable (QES) operator is [27–29]

$$\begin{aligned} H_{\text{qes}} = C_{++}J_n^+J_n^+ + C_{+0}J_n^+J_n^0 + C_{+-}J_n^+J_n^- + C_{0-}J_n^0J_n^- \\ + C_-J_n^-J_n^- + C_+J_n^+ + C_0J_n^0 + C_-J_n^- + C, \end{aligned} \tag{7}$$

in which the generators of $sl(2)$ are represented by these first-order differential operators:

$$J_n^+ = z^2\frac{d}{dz} - n\,z, \quad J_n^0 = z\frac{d}{dz} - \frac{n}{2}, \quad J_n^- = \frac{d}{dz}. \tag{8}$$

They satisfy the commutation relations

$$[J_n^+, J_n^-] = -2J_n^0, \quad \left[J_n^\pm, J_n^0\right] = \mp J_n^\pm, \tag{9}$$

and correspond thus to the oscillator representation of $sl(2)$ with Bargmann index $-n/2$. For a nonnegative integer n, any product of operators (8) leaves invariant the $(n+1)$-dimensional space of polynomials $\mathcal{P}_n[z] = \langle 1, z, z^2, \ldots, z^n\rangle$ with maximum order n because the ascending ladder operator J_n^+ annihilates z^n, which is therefore the highest weight vector of the $(2j+1)$-dimensional representation of $sl(2)$ with $j = n/2$. The constant function is annihilated by J_n^-, which is the lowest weight vector ($n = 0$ corresponds to the trivial representation with $J_0^{\pm,0}\langle 1\rangle = 0$). In other words, H_{qes} preserves the finite-dimensional space of polynomials of the form

$$\phi_n(z) = \sum_{m=0}^{n} d_m z^m. \tag{10}$$

Substituting Eq. (8) into Eq. (7), the operator H_{qes} is given by a second-order differential operator with polynomial coefficients:

$$H_{\text{qes}} = P_4(z)\frac{d^2}{dz^2} + P_3(z)\frac{d}{dz} + P_2(z),$$

in which

$$\begin{aligned} P_4(z) &= C_{++}z^4 + C_{+0}z^3 + C_{+-}z^2 + C_{0-}z + C_{--}, \\ P_3(z) &= C_{++}(2-2n)z^3 + \left(C_+ + C_{+0}\left(1 - \frac{3n}{2}\right)\right)z^2 \\ &\quad + (C_0 - nC_{+-})z + \left(C_- - \frac{n}{2}C_{0-}\right), \\ P_2(z) &= C_{++}n(n-1)z^2 + \left(\frac{n^2}{2}C_{+0} - nC_+\right)z + \left(C - \frac{n}{2}C_0\right). \end{aligned} \tag{11}$$

Now, when comparing Eq. (6) with Eq. (11), we find that if the constraint

$$\nu_0 = (n+1)\omega \tag{12}$$

is satisfied, then the Eq. (6) can be written as $\tilde{H}\phi_n(z) = 0$ and $\tilde{H}$ is given in terms of $J_n^{\pm}$:

$$\tilde{H} = J_n^+ J_n^- + \frac{\nu_1}{2\omega}(J_n^+ - J_n^-) + \frac{\gamma^2 - \nu_1^2}{4\omega^2}. \tag{13}$$

The condition (12) that fixes ν_0 in terms of ω and n is necessary to cancel terms proportional to z in Eq. (6) that cannot be absorbed into an expression containing J_n^+. Since $\tilde{H}$ leaves the space $\mathcal{P}_n[z]$ invariant, it can be expressed as a matrix $\tilde{H}_n$ of dimension $(n+1)\times(n+1)$. Using $v_0 = 1, v_1 = z, \ldots, v_n = z^n$ as a basis, we obtain the matrix elements of $J_n^{\pm}$ and $J_n^+ J_n^-$ from Eq. (8) as

$$\begin{aligned} J_n^+(i,j) &= -(n-j)\delta_{i,j+1}, \quad J_n^-(i,j) = j\delta_{i,j-1}, \\ J_n^+ J_n^-(i,j) &= (j-n-1)j\delta_{i,j}, \quad i,j = 0,\ldots,n. \end{aligned} \tag{14}$$

Therefore, $\tilde{H}_n$ is a tridiagonal matrix with elements

$$\begin{aligned} \tilde{H}_n(i,j) = &\left[(j-n-1)j + \frac{\gamma^2 - \nu_1^2}{4\omega^2}\right]\delta_{i,j} \\ &- \frac{\nu_1}{2\omega}[(n-j)\delta_{i,j+1} + j\delta_{i,j-1}]. \end{aligned} \tag{15}$$

The condition for the existence of a nontrivial solution of $\tilde{H}_n\phi_n = 0$ is $\det(\tilde{H}_n) = 0$, which implies a second condition that the parameters ν_1, γ, and ω must satisfy. We then present explicit solutions for $n = 0, 1, 2$ and subsequently the constraints on the determinants for n up to 5.

For $n = 0$, that is $\nu_0/\omega = 1$, we have $\phi_0(z) = d_0$ for which the equation $\tilde{H}_0\,\phi_0(z) = 0$ becomes $(\nu_1^2 - \gamma^2)d_0 = 0$. Thus, a nontrivial solution requires $\nu_1^2 = \gamma^2$, meaning that the driving amplitude ν_1 equals the gain/loss strength γ (both quantities can be chosen positive without loss of generality). This condition does not depend on the driving frequency ω, so this special solution does not imply a resonance phenomenon in the strict sense.

For $n = 1$, that is $\nu_0/\omega = 2$, we have for $\phi_1(z) = d_0 + d_1 z$ in the basis given above $\phi_1 = (d_0, d_1)^{\mathsf{T}}$ for which the equation $\tilde{H}_1\phi_1(z) = 0$ reads

$$\begin{pmatrix} \frac{\gamma^2-\nu_1^2}{4\omega^2} & -\frac{\nu_1}{2\omega} \\ -\frac{\nu_1}{2\omega} & \frac{\gamma^2-\nu_1^2}{4\omega^2} - 1 \end{pmatrix}\begin{pmatrix} d_0 \\ d_1 \end{pmatrix} = 0.$$

The condition $\det(\tilde{H}_1) = 0$ yields

$$\left(\nu_1^2 - \gamma^2\right)^2 = 4\omega^2\gamma^2, \tag{16}$$

and the coefficients d_0, d_1 satisfy

$$\frac{d_1}{d_0} = \frac{\gamma^2 - \nu_1^2}{2\omega\nu_1}.$$

We observe that in this case, the condition on ν_1 and γ involves the driving frequency ω, so it corresponds to a resonance between the gain/loss process and the driving. From Eq. (16), explicit solutions of ν_1^2/ω^2 are obtained as

$$\frac{\nu_1^2}{\omega^2} = \frac{\gamma^2}{\omega^2} \pm \frac{2\gamma}{\omega}.$$

For $n = 2$, meaning $\nu_0/\omega = 3$, the matrix equation $\tilde{H}_2\,\phi_2(z) = 0$ is

$$\begin{pmatrix} \frac{\gamma^2-\nu_1^2}{4\omega^2} & -\frac{\nu_1}{2\omega} & 0 \\ -\frac{\nu_1}{\omega} & \frac{\gamma^2-\nu_1^2}{4\omega^2} - 2 & -\frac{\nu_1}{\omega} \\ 0 & -\frac{\nu_1}{2\omega} & \frac{\gamma^2-\nu_1^2}{4\omega^2} - 2 \end{pmatrix}\begin{pmatrix} d_0 \\ d_1 \\ d_2 \end{pmatrix} = 0.$$

The determinant condition reads now

$$\left(\frac{\nu_1^2}{\omega^2} - \frac{\gamma^2}{\omega^2}\right)^3 - 16\left(\frac{\nu_1^2}{\omega^2} - \frac{\gamma^2}{\omega^2}\right)\frac{\gamma^2}{\omega^2} - 64\frac{\gamma^2}{\omega^2} = 0, \tag{17}$$

and, consequently, a nontrivial solution for the matrix equation is obtained as

$$\begin{aligned} d_1 &= \frac{4\omega\nu_1\left(\gamma^2 - \nu_1^2 - 8\omega^2\right)}{8\omega^2\left(\nu_1^2 - 2\gamma^2\right) + \left(\gamma^2 - \nu_1^2\right)^2 + 64\omega^4}\,d_0, \\ d_2 &= \frac{8\omega^2\nu_1^2}{8\omega^2\left(\nu_1^2 - 2\gamma^2\right) + \left(\gamma^2 - \nu_1^2\right)^2 + 64\omega^4}\,d_0. \end{aligned} \tag{18}$$

From Eq. (17), we obtain three solutions for $\frac{\nu_1^2}{\omega^2}$ in the form given by Cardano's formula, which are

$$\begin{aligned} \frac{\nu_1^2}{\omega^2} &= \left(1 + \frac{4}{\xi}\sqrt[3]{\frac{2}{3}}\right)\frac{\gamma^2}{\omega^2} + 2\left(\frac{2}{3}\right)^{2/3}\xi, \\ \frac{\nu_1^2}{\omega^2} &= \left(1 - \frac{4}{\xi}\sqrt[3]{-\frac{2}{3}}\right)\frac{\gamma^2}{\omega^2} + 2\left(-\frac{2}{3}\right)^{2/3}\xi, \\ \frac{\nu_1^2}{\omega^2} &= \left(1 + \frac{4}{\xi}(-1)^{2/3}\sqrt[3]{\frac{2}{3}}\right)\frac{\gamma^2}{\omega^2} - 2\sqrt[3]{-1}\left(\frac{2}{3}\right)^{2/3}\xi, \end{aligned}$$

where $\xi = \sqrt[3]{\frac{9\gamma^2}{\omega^2} + \frac{\sqrt{81\gamma^4\omega^2 - 12\gamma^6}}{\omega^3}}$.

Similarly, the determining conditions can be calculated for larger values of n. Let us summarize our results found explicitly for $n = 0, 1, \ldots, 5$, or equivalently, for $\frac{\nu_0}{\omega} = 1, 2, \ldots, 6$:

$$\begin{aligned} &\frac{\nu_0}{\omega} = 1 : \left(\frac{\nu_1^2}{\omega^2} - \frac{\gamma^2}{\omega^2}\right) = 0, \\ &\frac{\nu_0}{\omega} = 2 : \left(\frac{\nu_1^2}{\omega^2} - \frac{\gamma^2}{\omega^2}\right)^2 - 4\frac{\gamma^2}{\omega^2} = 0, \\ &\frac{\nu_0}{\omega} = 3 : \left(\frac{\nu_1^2}{\omega^2} - \frac{\gamma^2}{\omega^2}\right)^3 - 16\left(\frac{\nu_1^2}{\omega^2} - \frac{\gamma^2}{\omega^2}\right)\frac{\gamma^2}{\omega^2} - 64\frac{\gamma^2}{\omega^2} = 0, \\ &\frac{\nu_0}{\omega} = 4 : \left(\frac{\nu_1^2}{\omega^2} - \frac{\gamma^2}{\omega^2}\right)^4 - 40\left(\frac{\nu_1^2}{\omega^2} - \frac{\gamma^2}{\omega^2}\right)^2\frac{\gamma^2}{\omega^2} + 48\left(11\frac{\gamma^2}{\omega^2} - 8\frac{\nu_1^2}{\omega^2}\right)\frac{\gamma^2}{\omega^2} - 2304\frac{\gamma^2}{\omega^2} = 0, \end{aligned}$$

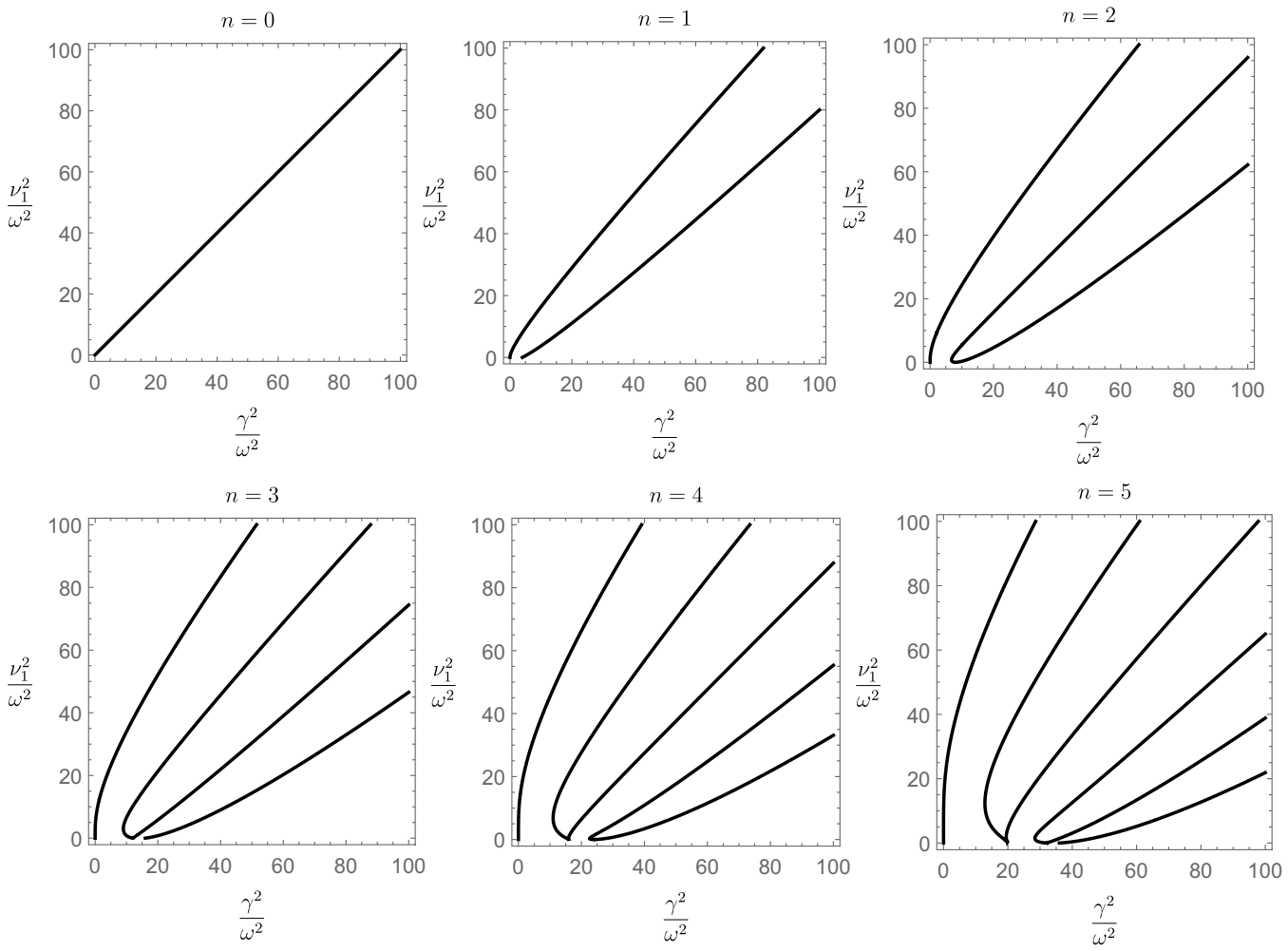

FIG. 1. The restrictions given by Eq. (19) for n photons, $n = 0, 1, 2, 3, 4$, and 5.

$$\frac{\nu_0}{\omega} = 5 : \left(\frac{\gamma^2}{\omega^2} - \frac{\nu_1^2}{\omega^2}\right)^5 - 80\left(\frac{\gamma^2}{\omega^2} - \frac{\nu_1^2}{\omega^2}\right)^3 \frac{\gamma^2}{\omega^2} + 64\left(\frac{37\gamma^4}{\omega^4} - \frac{58\gamma^2\nu_1^2}{\omega^2\omega^2} + \frac{21\nu_1^4}{\omega^4}\right)\frac{\gamma^2}{\omega^2}$$
$$- 6144\left(\frac{5\gamma^2}{\omega^2} - \frac{3\nu_1^2}{\omega^2}\right)\frac{\gamma^2}{\omega^2} + 147\,456\frac{\gamma^2}{\omega^2} = 0,$$
$$\frac{\nu_0}{\omega} = 6 : \left(\frac{\gamma^2}{\omega^2} - \frac{\nu_1^2}{\omega^2}\right)^6 - 140\left(\frac{\gamma^2}{\omega^2} - \frac{\nu_1^2}{\omega^2}\right)^4 \frac{\gamma^2}{\omega^2} + 112\left(\frac{69\gamma^2}{\omega^2} - \frac{32\nu_1^2}{\omega^2}\right)\left(\frac{\gamma^2}{\omega^2} - \frac{\nu_1^2}{\omega^2}\right)^2 \frac{\gamma^2}{\omega^2}$$
$$- 64\left(\frac{3281\gamma^4}{\omega^4} - \frac{4352\left(\gamma^2\nu_1^2\right)}{\omega^4} + \frac{1296\nu_1^4}{\omega^4}\right)\frac{\gamma^2}{\omega^2} + 20\,480\left(\frac{137\gamma^2}{\omega^2} - \frac{72\nu_1^2}{\omega^2}\right)\frac{\gamma^2}{\omega^2} - 14\,745\,600\frac{\gamma^2}{\omega^2} = 0. \quad (19)$$

We will now illustrate these conditions numerically in Fig. 1, and analyze how Floquet degeneracy varies with the modulation amplitude ν_1, loss/gain strength γ, and photon index $n' = n + 1 = 1, 2, \ldots$. Furthermore, in order to subsequently evaluate the time evolution of nearly degenerate Floquet states, we show in Fig. 3 the numerical results obtained from the 21-photon resonance condition, corresponding to $n = 20$ in Eq. (15). However, we do not report the explicit form of the condition in this case due to its large length and complexity, as it is the determinant condition of the 21×21 parametric matrix.

A. Numerical results and discussion

1. The n-photon constraints for n = 0, 1, 2, 3, 4, 5, and 20

The behavior of ν_1^2/ω^2 in terms of γ^2/ω^2, for the six conditions given in Eq. (19), is illustrated separately in Fig. 1. We observe that the general pattern of solution points starting with $n \geqslant 1$ is similar for all n with given parity (even or odd n) and large ν_1^2 and γ^2. This is illustrated in Fig. 2, where the solution sets for $(n_1, n_2) = (2, 4)$ and (3,5) are compared. The solution set for $n_1 < n_2$ is very close to a subset of the solutions for n_2 if ν_1^2 and γ^2 are sufficiently large. On the

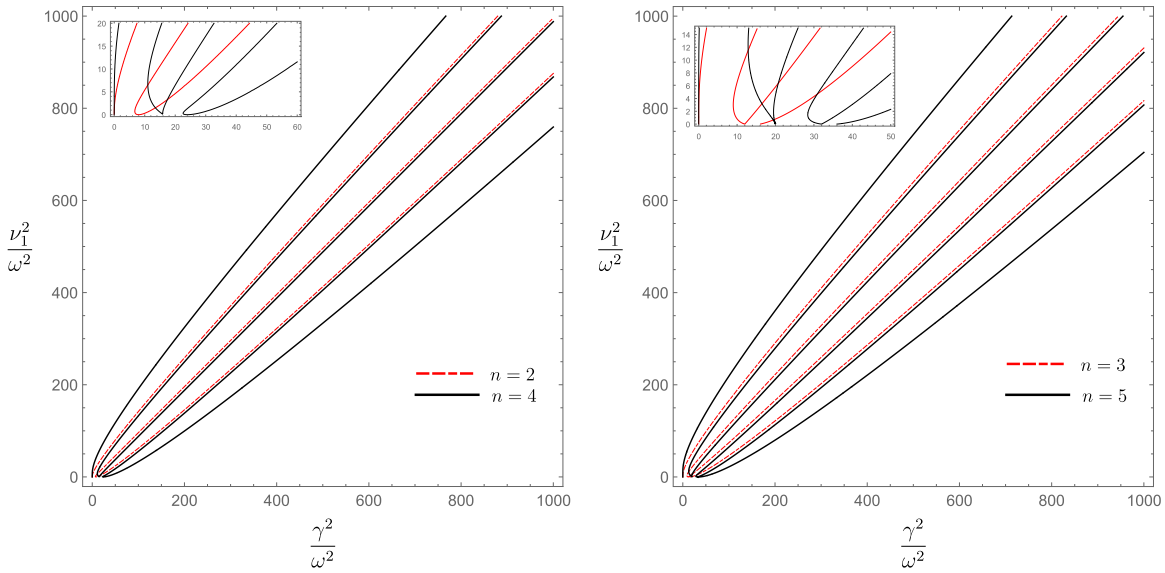

FIG. 2. The crossing points for doublets $(n_1, n_2) = (2, 4)$ on the left and $(n_1, n_2) = (3, 5)$ on the right.

other hand, for small ν_1^2, there are large deviations between the solution sets for n_1 and n_2, as shown in the insets in Fig. 2. For $\nu_1 = 0$ all solutions for γ^2 are obtained using the equations

$$(n + 1 - j)j = \gamma^2/(4\omega^2), \quad j = 0, \ldots, n. \tag{20}$$

This leads to doubly degenerate solutions for j and $j' = (n + 1 - j)$, which means that for this value of the gain/loss strength γ, there are two possible Floquet solutions with $\phi_1(t) = e^{ij\omega t}$ and $\phi_1(t) = e^{i(n+1-j)\omega t}$.

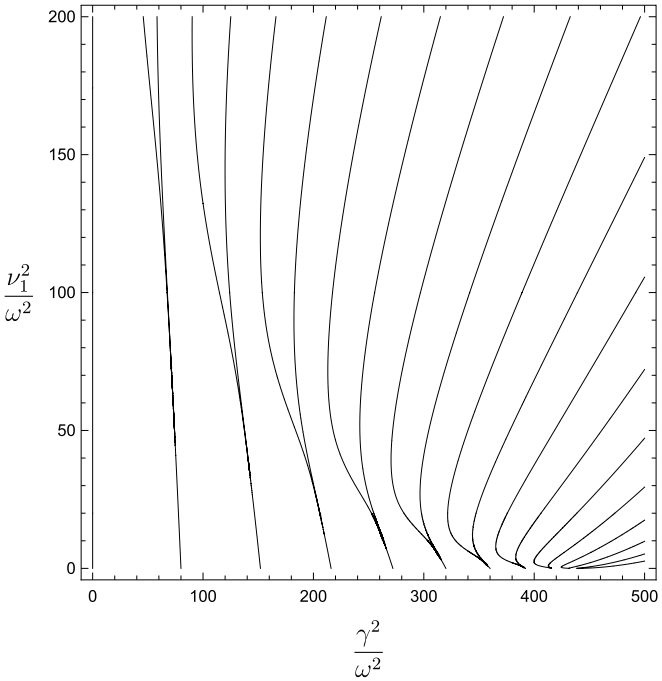

FIG. 3. Plot of the restriction of n photons for $n = 20$. Doubly degenerate solutions corresponding to the pairs $j = 1, \ldots, n$ and $j' = (n + 1 - j)$ in Eq. (20) occur for $\nu_1 = 0$ and $\frac{\gamma^2}{\omega^2} = \{80, 152, 216, 272, 320, 360, 392, 416, 432, 440\}$.

Our numerical results suggest that these degeneracies at the trivial point $\nu_1 = 0$ develop into two types for small but nonzero values of ν_1. In one case, the degenerate points diverge rapidly for $\nu_1^2 > 0$ as can be seen, for example, for $n = 2$ in Fig. 1. In the other case, the two solutions remain very close for $\nu_1^2 > 0$, implying quasidegeneracy even for nonzero ν_1. The "nearly degenerate" points are more clearly pronounced for pairs $(j, j') = (1, n)$ and large n, as can be seen in Fig. 3 for $n = 20$.

2. *Floquet quasienergy spectrum*

In this section, we numerically illustrate the behavior of the imaginary parts of the Floquet quasienergy spectrum of the $\mathcal{PT}$-symmetric Rabi model [Eq. (1)], as a function of ν_1/ω. We focus on two cases not reported in Ref. [26], namely the five- and six-photon resonances, corresponding to $n = 4$ and 5 in $\nu_0 = (n + 1)\omega$, respectively. Furthermore, we briefly describe the Floquet-theory-based procedure for time-periodic Hamiltonians [19,30–33]. We note that the Rabi model in Eq. (1) is time periodic, $H(t + T) = H(t)$, with $T = \frac{2\pi}{\omega}$. We begin with the Schrödinger equation [33],

$$i\frac{d}{dt}U(t) = H(t)U(t), \tag{21}$$

for the time-evolution operator $U(t)$, with initial condition $U(0) = \mathbb{1}$. Next, as a direct consequence of Floquet's theorem, it is easy to show that the Floquet modes satisfy the relation

$$U(T)\psi_j(0) = \mathrm{e}^{-i\varepsilon_j T}\psi_j(0), \quad j = 1, 2, \tag{22}$$

where $\psi_j(0)$ are the eigenvectors of the one-period propagator $U(T) = \hat{\mathcal{T}}\mathrm{e}^{-i\int_0^T H(t)\,dt}$, with $\hat{\mathcal{T}}$ being the time-ordering operator and ε_j the corresponding quasienergies. Therefore, the quasienergies ε_j are determined directly by taking the logarithm of the eigenvalues of the operator $U(T)$, multiplied by i/T. The matrix operator $U(T)$ is calculated numerically by solving the Schrödinger Eq. (21) for $U(t)$, $t \in [0, T]$,

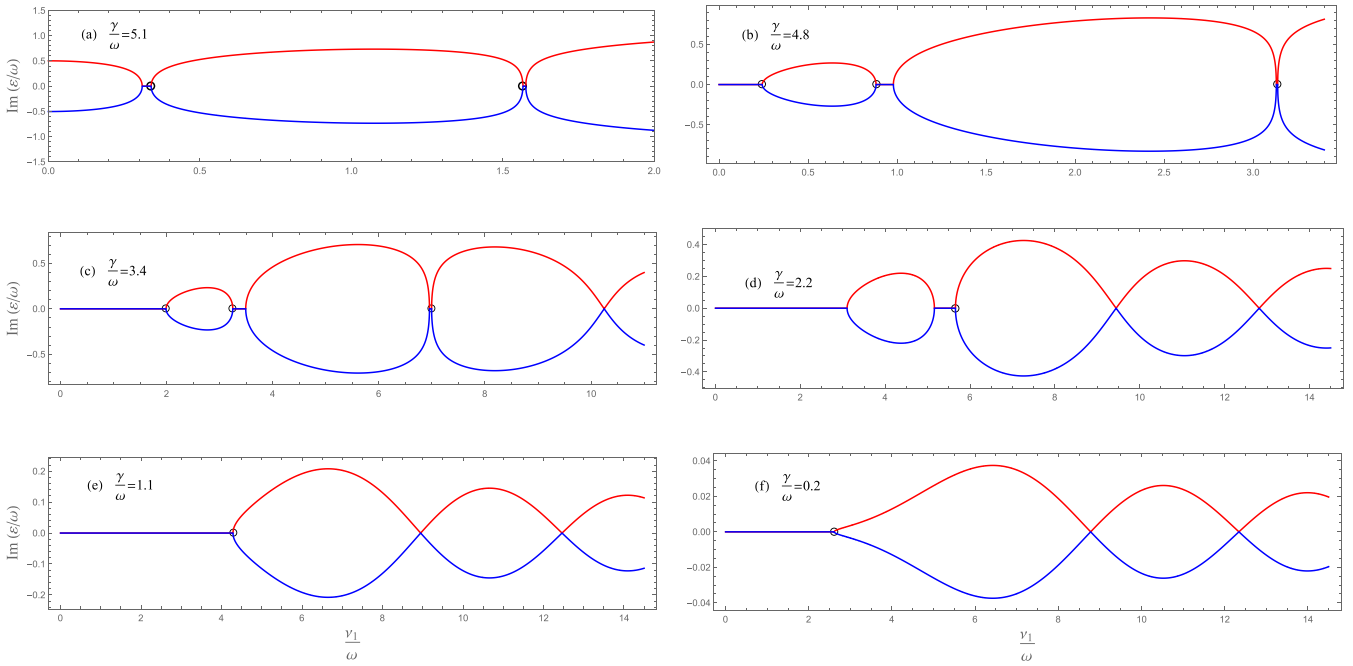

FIG. 4. Imaginary part of the Floquet quasienergies, $\mathrm{Im}(\varepsilon/\omega)$, as a function of ν_1/ω for $\nu_0 = 5\omega$ and different values of γ/ω. Without loss of generality, we fix $\omega = 1$. The circles represent the EPs corresponding to the exact Floquet solutions, identified numerically by the multiphoton condition (19) for $\nu_0/\omega = 5$. In (a), the EPs correspond to $\nu_1/\omega \approx 0.3391$ and 1.5664, in (b) to $\nu_1/\omega \approx 0.2423$, 0.8820, and 3.1381, in (c) to $\nu_1/\omega \approx 1.9887$, 3.2468, and 6.9949, in (d) to $\nu_1/\omega \approx 5.6552$, in (e) to $\nu_1/\omega \approx 4.2849$, and in (f) to $\nu_1/\omega \approx 2.6117$.

where $H(t) := H(t;\gamma,\nu_1)$ is the Rabi Hamiltonian in Eq. (1). The function `NDSolveValue` from `Mathematica 12` is used. For fixed value of γ/ω, the two eigenvalues of the operator $U(T)$ are computed for values of ν_1/ω ranging over the given interval, with step size of 0.001. In Figs. 4 and 5, we illustrate the imaginary parts of ε_j/ω as a function of the parameter ν_1/ω, for the parameter region corresponding to the five- and six-photon resonances. Without loss of generality, we fix $\omega = 1$. These figures show that at $\nu_1 = 0$, for $\frac{\gamma}{\omega} < \frac{\nu_0}{\omega}$ (respectively, $\frac{\gamma}{\omega} > \frac{\nu_0}{\omega}$), the $\mathcal{PT}$ symmetry is unbroken

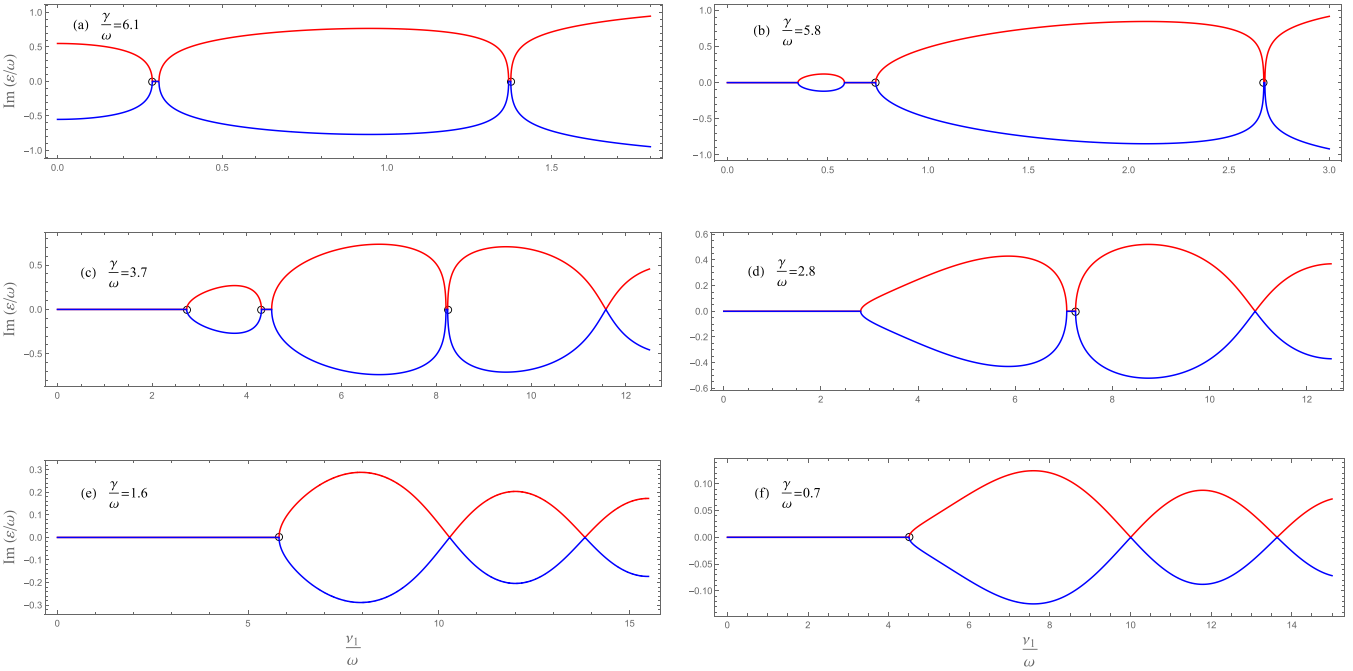

FIG. 5. The same as in Fig. 4, now for $\nu_0 = 6\omega$, where the circles indicating the EPs were identified numerically using the multiphoton relation (19) for $\nu_0/\omega = 6$: in (a) the EPs correspond to $\nu_1/\omega \approx 0.2879$ and 1.3762, in (b) $\nu_1/\omega \approx 0.7395$ and 2.6737, in (c) $\nu_1/\omega \approx 2.7280$, 4.3070, and 8.2392, in (d) $\nu_1/\omega \approx 7.2415$, in (e) $\nu_1/\omega \approx 5.8105$, and in (f) $\nu_1/\omega \approx 4.5058$.

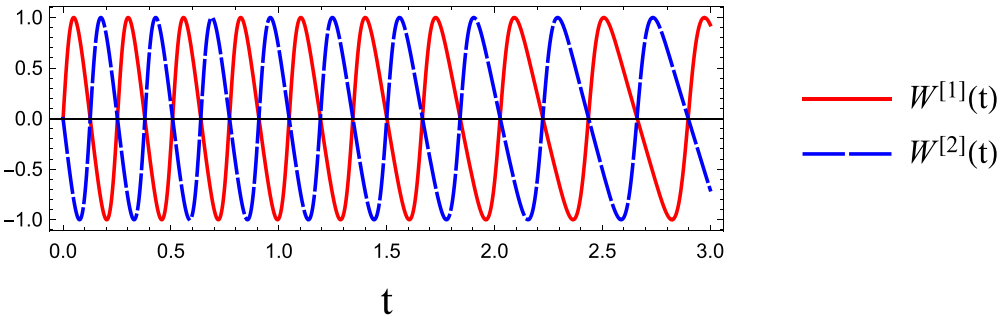

FIG. 6. Population inversions $W^{[\ell]}(t)$ corresponding to the nearly degenerate Floquet states $\psi^{[\ell]}(t)$, $\ell = 1, 2$, computed numerically for Example 1, ($\frac{\gamma^2}{\omega^2} \approx 76.5695$, $\frac{\nu_1^2}{\omega^2} = 30$) in Fig. 3 (numerical details given in Appendix A).

(respectively, it is broken) and the quasienergies are real with $\mathrm{Im}(\varepsilon/\omega) = 0$ [respectively, complex with $\mathrm{Im}(\varepsilon/\omega) \neq 0$]. This is due to the fact that at $\nu_1 = 0$, the time-dependent Hamiltonian (1) reduces to a static Hamiltonian $H = \frac{1}{2}\begin{pmatrix} i\gamma & \nu_0 \\ \nu_0 & -i\gamma \end{pmatrix}$, whose eigenvalues are given by $\pm\frac{1}{2}\sqrt{\nu_0^2 - \gamma^2}$. On the other hand, we see that as ν_1 increases, $\mathcal{PT}$ symmetry breaking becomes more pronounced, as indicated by the appearance of the EPs and loop structures in the quasienergy spectrum. $\mathcal{PT}$ symmetry breaking means that the Floquet quasienergies acquire imaginary parts and the system becomes unstable with one positive Lyapunov exponent. These are the "loops." The two quasienergies are real and different if the imaginary part vanishes and the system shows stable, quasiperiodic behavior. This is the $\mathcal{PT}$-symmetric phase. At the border of the $\mathcal{PT}$-symmetric phase, the two Floquet exponents become degenerate and the Floquet operator is no longer diagonalizable. These are the EPs. One of the time-dependent solutions is then quasiexact if γ is related to ν_1 by the two last conditions in Eq. (19) for $\nu_0/\omega = 5$, respectively $\nu_0/\omega = 6$.

3. *Time evolution of nearly degenerate Floquet states for n = 20*

In this section, we numerically evaluate the time evolution of population inversions for nearly degenerate Floquet states and their superposition. To this end, we focus on the case $n = 20$, whose 21-photon constraint was numerically illustrated in Fig. 3; here, we observe that at certain points $(\frac{\gamma^2}{\omega^2}, \frac{\nu_1^2}{\omega^2})$ in parameter space, the model exhibits a near degeneracy. In particular, the leftmost line in this figure splits into two branches above $\frac{\nu_1^2}{\omega^2} \approx 100$, and below this value the lines are nearly degenerate, $(\frac{\gamma^2}{\omega^2}, \frac{\nu_1^2}{\omega^2})^{[1]} \simeq (\frac{\gamma^2}{\omega^2}, \frac{\nu_1^2}{\omega^2})^{[2]}$. This means that for the parameter value $(\frac{\gamma^2}{\omega^2}, \frac{\nu_1^2}{\omega^2})^{[1]}$, not just one exact Floquet solution $(c_1^{[1]}(t), c_2^{[1]}(t))^{\mathsf{T}}$ exists but another solution $(c_1^{[2]}(t), c_2^{[2]}(t))^{\mathsf{T}}$ whose time development is very accurately described by the quasiexact solution corresponding to the minimally deviating parameter $(\frac{\gamma^2}{\omega^2}, \frac{\nu_1^2}{\omega^2})^{[2]}$. As the second solution has initial values linearly independent from the first, the time development of the complete qubit is exactly computable for this special parameter value if the resonance ratio ν_0/ω is sufficiently large.

The nearly degenerate points are determined numerically using the determinant condition $\det(\tilde{H}_{20}) = 0$, where the 21-dimensional matrix $\tilde{H}_{20}$ is given by Eq. (15). See Examples 1 and 2 below, and Appendix A for more numerical details. At the nearly degenerate point $(\frac{\gamma^2}{\omega^2}, \frac{\nu_1^2}{\omega^2})^{[1]}$, the matrix $\tilde{H}_{20}$ has a null vector with an exact zero eigenvalue, and an eigenvector associated with an almost-zero eigenvalue ϵ, which we denote by $\mathbf{d}^{[0]} := \mathbf{d}^{[1]}$ and $\mathbf{d}^{[\epsilon]} := \mathbf{d}^{[2]}$, respectively. These two sets $\mathbf{d}^{[\ell]}$, $\ell = 1, 2$ are introduced into the polynomial function $\phi(z)$ in Eq. (10) with $z(t) = e^{i\omega t}$, and we obtain the corresponding time-dependent functions $\phi^{[\ell]}(t) = \sum_{m=0}^{20} d_m^{[\ell]} e^{im\omega t}$. Now, we can proceed to the time evolution of the nearly degenerate Floquet states $\psi^{[\ell]}(t)$. The function $c_1^{[\ell]}(t)$ from Eq. (5) is now given explicitly by

$$c_1^{[\ell]}(t) = e^{\frac{\nu_1}{2\omega}\cos(\omega t)}\, e^{-\frac{i\nu_0 t}{2}} \sum_{m=0}^{20} d_m^{[\ell]}\, e^{im\omega t}.$$

On the other hand, using the equations of motion (2) and taking into account Eq. (3), the function $c_2^{[\ell]}(t)$ is easily de-

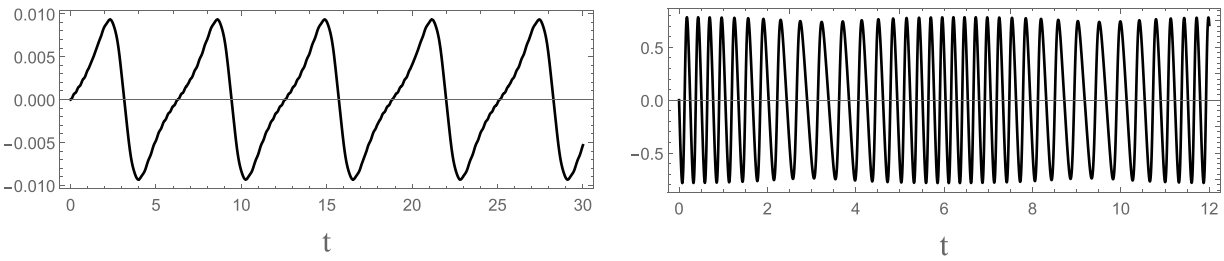

FIG. 7. Population inversion $W^{\mathrm{sup}}(t)$ for the state $\psi^{\mathrm{sup}}(t) = \alpha\,\psi^{[1]}(t) + \beta\,\psi^{[2]}(t)$ in Example 1. On the left for $\beta = \alpha = \frac{1}{\sqrt{2}}$, on the right for $\beta = 3\alpha = \frac{3}{\sqrt{10}}$.

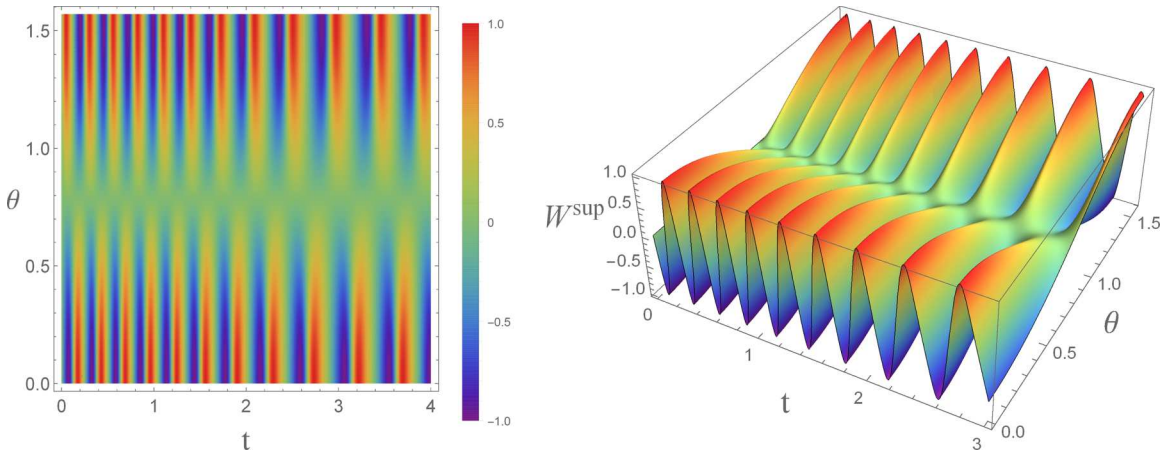

FIG. 8. $W^{\sup}(t)$ for the state $\psi^{\sup}(t) = \alpha\,\psi^{[1]}(t) + \beta\,\psi^{[2]}(t)$, $\alpha = \sin\theta$, and $\beta = \cos\theta$, in Example 1.

termined as a function of $c_1^{[\ell]}(t)$ as

$$c_2^{[\ell]}(t) = \frac{2}{\gamma}\left(\frac{d}{dt}c_1^{[\ell]}(t) - \frac{\nu(t)}{2i}c_1^{[\ell]}(t)\right).$$

Consequently, having determined $c_j^{[\ell]}(t)$, $j = 1, 2$, and making use of transformations (3), the "normalized" time-dependent Floquet states and the associated population inversions are given, respectively, by

$$\psi^{[\ell]}(t) = \left(\left|a_1^{[\ell]}(t)\right|^2 + \left|a_2^{[\ell]}(t)\right|^2\right)^{-\frac{1}{2}}\begin{pmatrix} a_1^{[\ell]}(t) \\ a_2^{[\ell]}(t)\end{pmatrix} = \begin{pmatrix}\psi_1^{[\ell]}(t) \\ \psi_2^{[\ell]}(t)\end{pmatrix}$$

and

$$W^{[\ell]}(t) = \left|\psi_1^{[\ell]}(t)\right|^2 - \left|\psi_2^{[\ell]}(t)\right|^2, \quad \ell = 1, 2. \tag{23}$$

We consider now an arbitrary superposition of these states,

$$\psi^{\sup}(t) = \alpha\,\psi^{[1]}(t) + \beta\,\psi^{[2]}(t) = \left(a_1^{\sup}(t), a_2^{\sup}(t)\right)^{\mathsf{T}},$$

where $\alpha, \beta \in \mathbb{C}$. Using the transformations (3), the components of the spinor c_j are

$$c_1^{\sup}(t) = \alpha\,c_1^{[1]}(t) + \beta\,c_1^{[2]}(t), \quad c_2^{\sup}(t) = \alpha\,c_2^{[1]}(t) + \beta\,c_2^{[2]}(t),$$

and consequently, the population inversion for the "normalized" superposition $\psi_{\mathcal{N}}^{\sup}(t) = (\psi_1^{\sup}(t), \psi_2^{\sup}(t))^{\mathsf{T}}$ is given by $W^{\sup}(t) = |\psi_1^{\sup}(t)|^2 - |\psi_2^{\sup}(t)|^2$. Next, we present the numerical results for $W^{[\ell]}(t)$ and $W^{\sup}(t)$ for two distinct almost degenerate points on the leftmost line of Fig. 3. Example 1 corresponds to the point ($\frac{\gamma^2}{\omega^2} \approx 76.5695$, $\frac{\nu_1^2}{\omega^2} = 30$), illustrated in Figs. 6–8.

Example 2 corresponds to the point ($\frac{\gamma^2}{\omega^2} \approx 71.6246$, $\frac{\nu_1^2}{\omega^2} = 70$), which is shown in Figs. 9–11. For the superposition coefficients, we use the parametrization $\alpha = \sin\theta$ and $\beta = \cos\theta$, with $\theta \in [0, \frac{\pi}{2}]$.

As a particular result, we observe that at $t = 0$, both nearly degenerate states $\psi^{[\ell]}(t)$, $\ell = 1, 2$, have zero population inversion, $W^{[\ell]}(0) \approx 0$, indicating that their "initial components" are equally populated. The relevant numerical data, including eigenvalues, eigenvectors, and spinor components, for Examples 1 and 2, are provided in detail in Appendix A.

III. CONCLUSIONS

In this work, we considered the algebraic structure of a special $\mathcal{PT}$-symmetric semiclassical Rabi model. It turns out that the condition for the existence of a finite-dimensional invariant subspace has the form of a resonance condition between the driving frequency and the constant term of the driving: $\nu_0/\omega = n + 1$. The time-dependent Schrödinger equation then has a quasiexact solution corresponding to a so-called EPs at the edge of the $\mathcal{PT}$-symmetric region in parameter space [26]. The invariant subspace belongs to the spin-$(n/2)$ representation of $sl(2)$ [27], since the time-dependent Hamiltonian can be written in terms of $sl(2)$

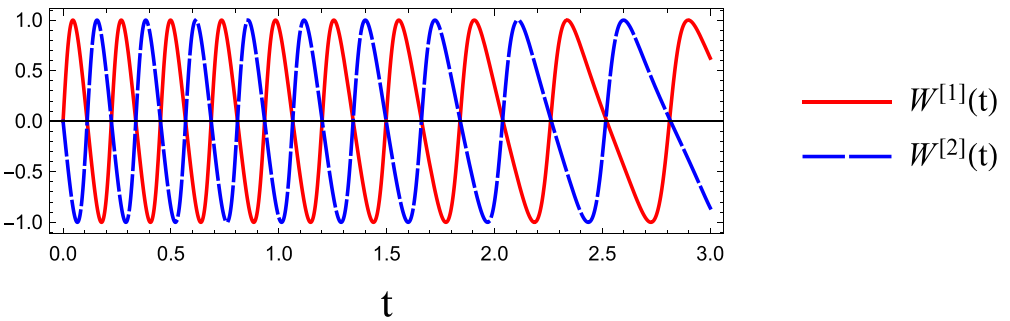

FIG. 9. Population inversions $W^{[\ell]}(t)$ corresponding to the nearly degenerate Floquet states $\psi^{[\ell]}(t)$, $\ell = 1, 2$, computed numerically for Example 2, ($\frac{\gamma^2}{\omega^2} \approx 71.6246$, $\frac{\nu_1^2}{\omega^2} = 70$) in Fig. 3 (see numerical details in Appendix A).

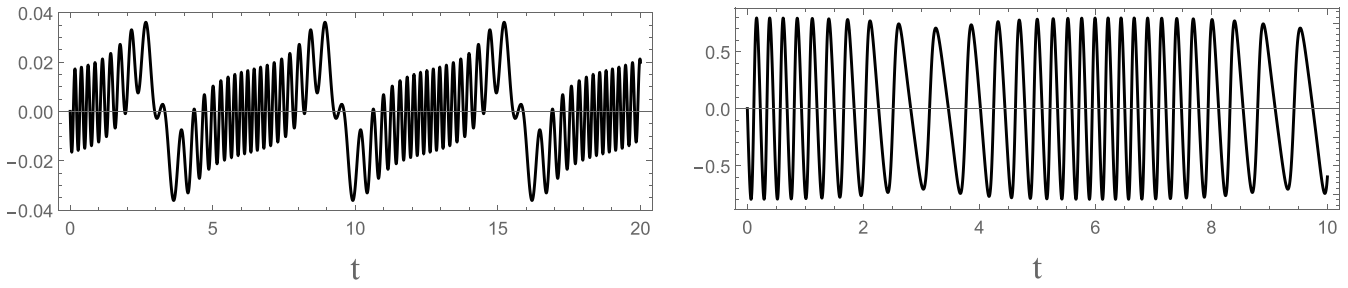

FIG. 10. Population inversion $W^{\mathrm{sup}}(t)$ for the state $\psi^{\mathrm{sup}}(t) = \alpha\,\psi^{[1]}(t) + \beta\,\psi^{[2]}(t)$ in Example 2. On the left for $\beta = \alpha = \frac{1}{\sqrt{2}}$, on the right for $\beta = 3\alpha = \frac{3}{\sqrt{10}}$.

generators acting in this representation. This allows to give determinant expressions for the additional relation between the driving strength ν_1 and the dissipative coupling γ in closed form. The trivial representation $n = 0$ is a special case, in which the gain/loss term exactly balances the driving and leads to the simplest type of exceptional point. The quasiexact solution is usually unique for a given parameter set $\{\nu_0/\omega, \nu_1/\omega, \gamma/\omega\}$, with the exception of the case with time-independent driving, $\nu_1 = 0$, where two Floquet solutions exist. Interestingly, some of the two possible Floquet solutions for fixed gain/loss γ continue to exist approximately with high accuracy for $\nu_1 \neq 0$ if the quotient ν_0/ω is a large integer. This means that the full two-level system has an exactly known time evolution, which could be of use for applications in quantum information technology employing driven qubits with balanced gain and loss.

We observe that Eq. (6) belongs to the class of double confluent Heun equations [34]. It has two irregular singular points of s-rank two at $z = 0$ and $z = \infty$, which are created by a confluence of two pairs of regular singular points (the same class is sometimes called 'biconfluent' [35,36]). If the exponents of second kind vanish both at $z = 0$ and $z = \infty$, and therefore allow a Frobenius expansion of the solution around $z = 0$, it can be expressed as a polynomial in z if certain constraints on the parameters are satisfied [35,36]. These restrictions are reduced in our case to the condition (12) and the annulment of the determinant of the matrix (15).

It seems that the class of $\mathcal{PT}$-symmetric systems contains other QES models that provide a deeper understanding of the solution structure. We are working to conduct a fairly comprehensive study of this interesting exploration.

ACKNOWLEDGMENTS

The authors would like to thank the anonymous referees for their valuable comments, which helped improve the quality of the manuscript. The work of M.B. was supported by the Czech Science Foundation under Project No. 22-18739S. D.B. was funded by the Deutsche Forschungsgemeinschaft (DFG, German Research Foundation), Grant No. 439943572. The research of L.M.N. and S.Z. was supported by the Q-CAYLE project, funded by the European Union-Next Generation UE/MICIU/Plan de Recuperacion, Transformacion y Resiliencia/Junta de Castilla y Leon (PRTRC17.11), and also by project PID2023-148409NB-I00, funded by MICIU/AEI/10.13039/501100011033; financial support of the Department of Education of the Junta de Castilla y Leon and FEDER Funds is also gratefully acknowledged (reference: CLU-2023-1-05). M.B. is grateful to A.V. Turbiner for helpful discussions during the preparation of this manuscript.

DATA AVAILABILITY

No data were created or analyzed in this study.

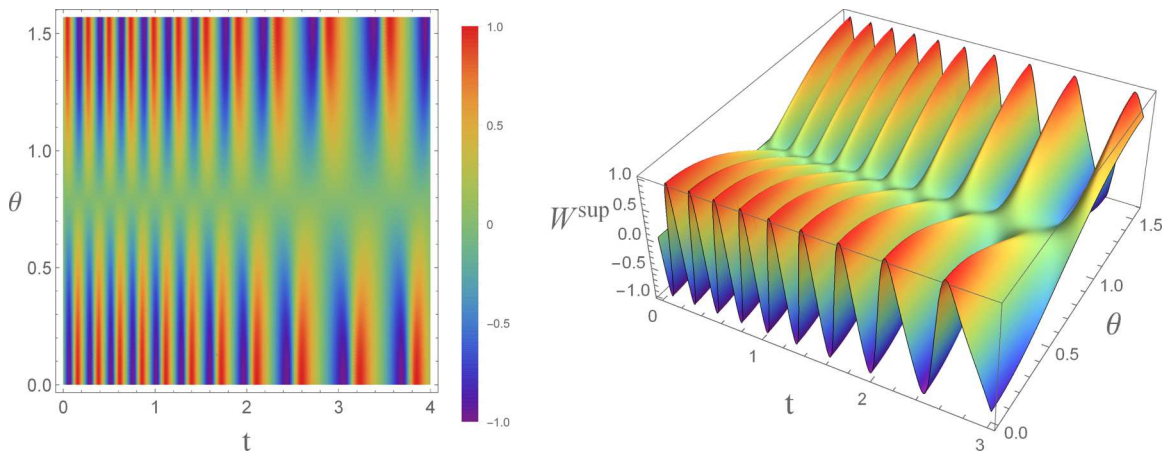

FIG. 11. $W^{\mathrm{sup}}(t)$ for the state $\psi^{\mathrm{sup}}(t) = \alpha\,\psi^{[1]}(t) + \beta\,\psi^{[2]}(t)$, $\alpha = \sin\theta$, and $\beta = \cos\theta$, in Example 2.

APPENDIX A: NUMERICAL DATA FOR TIME EVOLUTION OF NEARLY DEGENERATE FLOQUET STATES FOR $n = 20$

In this Appendix, we provide the relevant numerical data supporting the figures and discussion in Examples 1 and 2 in Sec. II A 3, which were used to evaluate the population inversions of the nearly degenerate Floquet states for $n = 20$. All computations performed using `Mathematica 12` with 100 digits of precision; the results presented here are duly rounded.

1. Example 1: Nearly degenerate point ($\frac{\gamma^2}{\omega^2} \approx 76.5695$, $\frac{\nu_1^2}{\omega^2} = 30$) in Fig. 3

The results for this example are presented in Figs. 6–8. First, it should be mentioned that the rounded value of the parameter $\frac{\gamma^2}{\omega^2} \approx 76.5695$ was used in our calculations as a symbolic representation of the second root of a polynomial of degree 21 in the form of

$$\text{Root}[-10\,460\,353\,203\,000\,000\,000\,000\,000\,000\,000 + \cdots + 215\,839\,12x^{19} - 6790x^{20} + x^{21}, 2],$$

as a `Root` object in `Mathematica 12`, which was determined numerically using the determinant condition $\det(\tilde{H}_{20}) = 0$. As mentioned in Sec. II A 3, at any fixed pair $(\frac{\gamma^2}{\omega^2}, \frac{\nu_1^2}{\omega^2})$ located on a nearly degenerate line in Fig. 3, matrix $\tilde{H}_{20}$ has a null vector corresponding to the exact zero eigenvalue (denoted by $\mathbf{d}^{[1]}$) and an eigenvector associated with an almost-zero eigenvalue ϵ (denoted by $\mathbf{d}^{[2]}$). In this example, the almost-zero eigenvalue is $\epsilon \approx -3.155 \times 10^{-6}$, and the eigenvectors $\mathbf{d}^{[\ell]}$, $\ell = 1, 2$, are the following:

$$\mathbf{d}^{[1]} \approx \begin{pmatrix} -0.020\,353\,4915 \\ -0.086\,526\,6915 \\ 0.335\,564\,7364 \\ -0.528\,538\,6941 \\ 0.533\,661\,3134 \\ -0.399\,400\,2305 \\ 0.238\,452\,9392 \\ -0.118\,807\,0667 \\ 0.051\,005\,3685 \\ -0.019\,513\,9025 \\ 0.007\,452\,8874 \\ -0.004\,819\,8592 \\ 0.008\,214\,7473 \\ -0.018\,896\,5950 \\ 0.040\,825\,3726 \\ -0.077\,005\,6234 \\ 0.122\,396\,5468 \\ -0.157\,063\,0643 \\ 0.152\,366\,5430 \\ -0.099\,233\,4752 \\ 0.032\,516\,6852 \end{pmatrix}, \quad \mathbf{d}^{[2]} \approx \begin{pmatrix} 0.020\,355\,0543 \\ 0.086\,533\,3588 \\ -0.335\,590\,4883 \\ 0.528\,578\,9548 \\ -0.533\,700\,9539 \\ 0.399\,426\,3730 \\ -0.238\,455\,9100 \\ 0.118\,763\,1507 \\ -0.050\,827\,0501 \\ 0.018\,909\,1468 \\ -0.005\,539\,0449 \\ -0.000\,824\,1033 \\ 0.007\,082\,3516 \\ -0.018\,598\,0293 \\ 0.040\,753\,2473 \\ -0.076\,993\,3274 \\ 0.122\,401\,5998 \\ -0.157\,074\,0918 \\ 0.152\,378\,0174 \\ -0.099\,241\,0654 \\ 0.032\,519\,1847 \end{pmatrix},$$

which are approximately half symmetric and half antisymmetric. The angle between the vectors is easily computed as $\vartheta \approx 2.561\,528$ rad, confirming numerically that vectors are far from being parallel or antiparallel. As observed in Fig. 6, the initial population inversion of each nearly degenerate Floquet state is almost zero: $W^{[1]}(0) \approx W^{[2]}(0) \approx 0$. The corresponding numerical data at $t = 0$ are

$$\phi^{[1]}(0) \approx -0.007\,701\,5541, \quad \phi^{[2]}(0) \approx 0.010\,856\,3748,$$

$$c_1^{[1]}(0) \approx -0.119\,108\,5102, \quad c_2^{[1]}(0) \approx 0.119\,108\,5102\,i,$$

$$c_1^{[2]}(0) \approx 0.167\,899\,4402, \quad c_2^{[2]}(0) \approx 0.167\,899\,4540\,i,$$

$$a_1^{[1]}(0) \approx -0.119\,108\,5102 + 0.119\,108\,5102\,i, \quad a_2^{[1]}(0) \approx -0.119\,108\,510\,2 - 0.119\,108\,5102\,i,$$

$$a_1^{[2]}(0) \approx 0.167\,899\,4402 + 0.167\,899\,4540\,i, \quad a_2^{[2]}(0) \approx 0.167\,899\,440\,2 - 0.167\,899\,4540\,i.$$

Accordingly, the "normalized" nearly degenerate states are determined as

$$\psi^{[1]}(0) \approx \begin{pmatrix} -0.5 + 0.5\,i \\ -0.5 - 0.5\,i \end{pmatrix}, \quad \psi^{[2]}(0) \approx \begin{pmatrix} 0.499\,999\,9794 + 0.500\,000\,0206\,i \\ 0.499\,999\,9794 - 0.500\,000\,0206\,i \end{pmatrix},$$

which obviously confirm the almost-zero initial population inversions of each state. On the other hand, the inner product of the vectors $\psi^{[\ell]}(0)$ and the angle between them are, respectively, computed as $\langle \psi^{[1]}(0) \,|\, \psi^{[2]}(0) \rangle \approx 4.1204 \times 10^{-8} \approx 0$ and

$\tilde{\vartheta} \approx 1.570\,796$ rad $\approx \frac{\pi}{2}$, indicating that the nearly degenerate states $\psi^{[1]}(0)$ and $\psi^{[2]}(0)$ are indeed almost orthogonal and linearly independent.

2. Example 2: Nearly degenerate point ($\frac{\gamma^2}{\omega^2} \approx 71.6246$, $\frac{\nu_1^2}{\omega^2} = 70$) in Fig. 3

The results corresponding to this example are illustrated in Figs. 9–11. Let us mention, again, that the rounded parameter value $\frac{\gamma^2}{\omega^2} \approx 71.6246$ was used in our computation as a symbolic representation of an algebraic number in the form of

$$\text{Root}[-558\,545\,864\,083\,284\,007\,000\,000\,000\,000\,000\,000\,000 + \cdots + 27\,105\,512x^{19} - 7630x^{20} + x^{21}, 2],$$

as a `Root` object in `Mathematica 12`, which was determined numerically using the determinant condition $\det(\tilde{H}_{20}) = 0$. In this case, the almost-zero eigenvalue is $\epsilon \approx -0.004\,5225$, and the eigenvectors $\mathbf{d}^{[\ell]}$ are

$$\mathbf{d}^{[1]} \approx \begin{pmatrix} -0.008\,022\,9890 \\ -0.000\,778\,9301 \\ 0.082\,054\,0768 \\ -0.240\,863\,8702 \\ 0.402\,206\,3995 \\ -0.480\,834\,7967 \\ 0.452\,222\,4593 \\ -0.353\,248\,4265 \\ 0.238\,744\,6380 \\ -0.146\,662\,5957 \\ 0.090\,720\,4408 \\ -0.069\,400\,0277 \\ 0.075\,911\,1251 \\ -0.102\,140\,1965 \\ 0.137\,291\,2067 \\ -0.165\,862\,6138 \\ 0.170\,533\,5595 \\ -0.142\,079\,7483 \\ 0.089\,644\,0796 \\ -0.038\,011\,8567 \\ 0.008\,115\,5549 \end{pmatrix}, \qquad \mathbf{d}^{[2]} \approx \begin{pmatrix} 0.008\,160\,5886 \\ 0.000\,801\,1116 \\ -0.083\,481\,5872 \\ 0.244\,969\,4825 \\ -0.408\,866\,0361 \\ 0.488\,308\,6216 \\ -0.458\,075\,6536 \\ 0.355\,070\,6308 \\ -0.233\,767\,4304 \\ 0.130\,307\,5629 \\ -0.054\,614\,1023 \\ -0.000\,242\,2858 \\ 0.046\,040\,6791 \\ -0.090\,917\,6190 \\ 0.134\,502\,1422 \\ -0.166\,752\,3105 \\ 0.172\,759\,1078 \\ -0.144\,297\,9423 \\ 0.091\,132\,0483 \\ -0.038\,659\,7426 \\ 0.008\,255\,7845 \end{pmatrix}.$$

The angle between the vectors in this case is $\vartheta \approx 2.432\,619$ rad. As in the previous example, it is observed in Fig. 9 that the initial population inversions are almost zero for both nearly degenerate states, $W^{[\ell]}(0) \approx 0$. The relevant numerical data at $t = 0$ are the following:

$$\phi^{[1]}(0) \approx -0.000\,462\,5107, \quad \phi^{[2]}(0) \approx 0.000\,633\,0503,$$
$$c_1^{[1]}(0) \approx -0.030\,332\,3440, \quad c_2^{[1]}(0) \approx 0.030\,332\,3440\,i,$$
$$c_1^{[2]}(0) \approx 0.041\,516\,6595, \quad c_2^{[2]}(0) \approx 0.041\,521\,9021\,i,$$
$$a_1^{[1]}(0) \approx -0.030\,332\,344\,0 + 0.030\,332\,3440\,i, \quad a_2^{[1]}(0) \approx -0.030\,332\,344\,0 - 0.030\,332\,3440\,i,$$
$$a_1^{[2]}(0) \approx 0.041\,516\,659\,5 + 0.041\,521\,9021\,i, \quad a_2^{[2]}(0) \approx 0.041\,516\,659\,5 - 0.041\,521\,9021\,i.$$

The "normalized" nearly degenerate states are accordingly determined as

$$\psi^{[1]}(0) \approx \begin{pmatrix} -0.5 + 0.5\,i \\ -0.5 - 0.5\,i \end{pmatrix}, \quad \psi^{[2]}(0) \approx \begin{pmatrix} 0.499\,968\,4320 + 0.500\,031\,5660\,i \\ 0.499\,968\,4320 - 0.500\,031\,5660\,i \end{pmatrix},$$

confirming, obviously, the almost-zero initial population inversions. The inner product of the vectors $\psi^{[\ell]}(0)$ and the angle between them are, respectively, computed as $\langle \psi^{[1]}(0) \,|\, \psi^{[2]}(0) \rangle \approx 0.000\,063\,13 \approx 0$ and $\tilde{\vartheta} \approx 1.570\,7332$ rad $\approx \frac{\pi}{2}$, indicating, again, that the nearly degenerate states are almost orthogonal and linearly independent at $t = 0$.

APPENDIX B: EFFECTIVE AND QES POTENTIALS ASSOCIATED WITH THE MODEL

In this Appendix, we analyze the Schrödinger-like potentials associated with the Rabi model in its original form [Eq. (6)], and in its $sl(2)$ Lie-algebraic form, Eq. (13). We begin with the first case. Using the equivalence problem for second-order differential operators [29], the Eq. (6) can be transformed into a Schrödinger-like equation. We do not analyze the rigorous spectral equivalence of the operators in terms of the boundary conditions here, as that is beyond the scope of this study. Let us

first consider $\mathscr{H}\Psi(z) = 0$ with

$$-\mathscr{H} = \mathcal{P}(z)\frac{d^2}{dz^2} + \mathcal{Q}(z)\frac{d}{dz} + \mathcal{R}(z),$$

and $\mathcal{P}(z) > 0$. Then using the change of variable

$$x = \varphi(z) = \int^z \frac{dy}{\sqrt{\mathcal{P}(y)}}, \tag{B1}$$

and the gauge factor $\mu(z) = |\mathcal{P}(z)|^{-\frac{1}{4}} \exp\{\int^z \frac{\mathcal{Q}(y)}{2\mathcal{P}(y)}dy\}$, we arrive at $\mu(z)\,\mathscr{H}\,\frac{1}{\mu(z)} = -\frac{d^2}{dx^2} + V(x)$, in which the potential has the form

$$V(x) = \left\{\frac{3\mathcal{P}'^2(z) - 8\mathcal{Q}(z)\mathcal{P}'(z) + 4\mathcal{Q}^2(z)}{16\mathcal{P}(z)} - \mathcal{R}(z) + \frac{1}{2}\mathcal{Q}'(z) - \frac{1}{4}\mathcal{P}''(z)\right\}\Big|_{z=\varphi^{-1}(x)}. \tag{B2}$$

The corresponding Schrödinger wave function is then given by $\tilde{\Psi}(x) = \mu(\varphi^{-1}(x))\Psi(\varphi^{-1}(x))$. In our case, from Eq. (6), we get

$$\begin{aligned}
\mathcal{P}(z) &= z^2,\\
\mathcal{Q}(z) &= \frac{\nu_1}{2\omega}z^2 + \Big(1 - \frac{\nu_0}{\omega}\Big)z - \frac{\nu_1}{2\omega},\\
\mathcal{R}(z) &= \frac{\gamma^2 - \nu_1^2}{4\omega^2} + \frac{\nu_1}{2\omega}\Big(1 - \frac{\nu_0}{\omega}\Big)z,
\end{aligned}$$

from which, together with Eq. (B1), we obtain $z = e^x$. The corresponding Schrödinger-like potential (B2) is then explicitly obtained as

$$\begin{aligned}
V(x) &= \left(\frac{\nu_1^2 - 2\gamma^2 + 2\nu_0^2}{8\omega^2} + \frac{\nu_1^2 z^2}{16\omega^2} + \frac{\nu_1^2}{(16\omega^2)z^2} + \frac{\nu_1(\nu_0 - \omega)z}{4\omega^2} + \frac{\nu_1(\nu_0 + \omega)}{(4\omega^2)z}\right)\Big|_{z=e^x}\\
&= \frac{\nu_1^2 - 2\gamma^2 + 2\nu_0^2 + \nu_1(4\nu_0\cosh x + \nu_1\cosh 2x - 4\omega\sinh x)}{8\omega^2}.
\end{aligned}$$

Recalling $z = e^{i\omega t}$, the obtained potential simplifies to

$$V_{\rm eff}(t) = \frac{\nu_1^2 - 2\gamma^2 + 2\nu_0^2 + \nu_1(4\nu_0\cos(\omega t) + \nu_1\cos(2\omega t))}{8\omega^2} - i\,\frac{\nu_1}{2\omega}\sin(\omega t). \tag{B3}$$

It is easily checked that $V(-t) = V^*(t)$, which reflects the $\mathcal{PT}$-symmetric structure of the underlying Hamiltonian.

In a similar way, by applying the outlined method to the Rabi model in its $sl(2)$ Lie-algebraic form [Eq. (13)], one obtains the following associated QES potential [27,29]:

$$V_{\rm qes}(t) = \frac{\nu_1^2 - 2\gamma^2 + 2(n+1)^2\omega^2 + \nu_1(4(n+1)\omega\cos(\omega t) + \nu_1\cos(2\omega t))}{8\omega^2} - i\,\frac{\nu_1}{2\omega}\sin(\omega t),$$

which explicitly depends on the parameter n, dimension of the invariant subspace of polynomials. As a result, a finite part of the spectrum, the first $n+1$ solutions, can be computed algebraically (as discussed in Sec. II). As can be seen, $V_{\rm qes}(t)$ coincides with the effective potential (B3), taking into account the quasiexact solvability constraint (12), i.e., $\nu_0 = (n+1)\omega$. The obtained potential visually resembles the $\mathcal{PT}$-symmetric periodic Khare-Mandal or complex Razavy potential, discussed in Ref. [37].

[1] C. M. Bender and S. Boettcher, Real spectra in non-Hermitian Hamiltonians having $\mathcal{PT}$ symmetry, Phys. Rev. Lett. **80**, 5243 (1998).

[2] C. M. Bender and D. W. Hook, PT-symmetric quantum mechanics, Rev. Mod. Phys. **96**, 045002 (2024).

[3] C. E. Rüter, *et al.*, Observation of parity–time symmetry in optic, Nat. Phys. **6**, 192 (2010).

[4] V. V. Konotop, J. Yang, and D. A. Zezyulin, Nonlinear waves in PT-symmetric systems, Rev. Mod. Phys. **88**, 035002 (2016).

[5] L. Chang, *et al.*, Parity–time symmetry and variable optical isolation in active–passive-coupled microresonators, Nat. Photon **8**, 524 (2014).

[6] B. Peng, *et al.*, Parity–time-symmetric whispering-gallery microcavities, Nat. Phys. **10**, 394 (2014).

[7] Y. Ashida, S. Furukawa, and M. Ueda, Parity-time-symmetric quantum critical phenomena, Nat. Commun. **8**, 15791 (2017).

[8] S. Assawaworrarit, X. Yu, and Sh Fan, Robust wireless power transfer using a nonlinear parity–time-symmetric circuit, Nature (London) **546**, 387 (2017).

[9] L. Xiao, *et al.*, Observation of topological edge states in parity–time-symmetric quantum walks, Nat. Phys. **13**, 1117 (2017).

[10] S. Weimann, *et al.*, Topologically protected bound states in photonic parity–time-symmetric crystals, Nat. Mater. **16**, 433 (2017).

[11] P.-Y. Chen, *et al.*, Generalized parity–time symmetry condition for enhanced sensor telemetry, Nat. Electron. **1**, (2018) 297.

[12] S. Assawaworrarit and Sh Fan, Robust and efficient wireless power transfer using a switch-mode implementation of a nonlinear parity–time symmetric circuit, Nat. Electron. **3**, 273 (2020).
[13] W. Cao, *et al.*, Fully integrated parity–time-symmetric electronics, Nat. Nanotechnol. **17**, 262 (2022).
[14] W. Liu, *et al.*, Floquet parity-time symmetry in integrated photonics, Nat. Commun. **15**, 946 (2024).
[15] A. Fritzsche, *et al.*, Parity–time-symmetric photonic topological insulator, Nat. Mater. **23**, 377 (2024).
[16] I. I. Rabi, Space quantization in a gyrating magnetic field, Phys. Rev. **51**, 652 (1937).
[17] Q. Xie, *et al.*, The quantum Rabi model: Solution and dynamics, J. Phys. A: Math. Theor. **50**, 113001 (2017).
[18] T. E. Lee and Y. N. Joglekar, PT-symmetric Rabi model: Perturbation theory, Phys. Rev. A **92**, 042103 (2015).
[19] J. Gong and Q. H. Wang, Stabilizing non-Hermitian systems by periodic driving, Phys. Rev. A **91**, 042135 (2015).
[20] J. Li, *et al.*, Observation of parity-time symmetry breaking transitions in a dissipative Floquet system of ultracold atoms, Nat. Commun. **10**, 855 (2019).
[21] Y. Liu, L. Mao, and Y. Zhang, Floquet analysis of extended Rabi models based on high-frequency expansion, Phys. Rev. A **105**, 053717 (2022).
[22] X. Lu, H. Li, J. K. Shi, L. B. Fan, V. Mangazeev, Z. M. Li, and M. T. Batchelor, PT-symmetric quantum Rabi model, Phys. Rev. A **108**, 053712 (2023).
[23] L. Guo, M. Marthaler, and G. Schön, Phase space crystals: A new way to create a quasienergy band structure, Phys. Rev. Lett. **111**, 205303 (2013).
[24] S. Mundhada, *et al.*, Encoding a qubit in an oscillator, Phys. Rev. Appl. **12**, 054051 (2019).
[25] C. W. S. Chang, C. Sabin, P. Forn Díaz, F. Quijandria, A. M. Vadiraj, I. Nsanzineza, G. Johansson, and C. M. Wilson, Observation of three-photon spontaneous parametric down-conversion in a superconducting parametric cavity, Phys. Rev. X **10**, 011011 (2020).
[26] Q. Xie, Sh Rong, and X. Liu, Exceptional points in a time-periodic parity-time-symmetric Rabi model, Phys. Rev. A **98**, 052122 (2018).
[27] A. Turbiner, Quasi-exactly-solvable problems and $sl(2)$ algebra, Commun. Math. Phys. **118**, 467 (1988).
[28] A. V. TurbinerOne-dimensional quasi-exactly solvable Schrödinger equations, Phys. Rep. **642**, 1 (2016).
[29] A. Gonzalez-Lopez, N. Kamran, and P. J. Olver, Quasi-exact solvability, Contemp. Math. **160**, 113 (1994).
[30] J. H. Shirley, Solution of the Schrödinger equation with a Hamiltonian periodic in time, Phys. Rev. **138**, B979 (1965).
[31] H. Sambe, Steady states and quasienergies of a quantum-mechanical system in an oscillating field, Phys. Rev. A **7**, 2203 (1973).
[32] B. Höckendorf, A. Alvermann, and H. Fehske, Topological origin of quantized transport in non-Hermitian Floquet chains, Phys. Rev. Res. **2**, 023235 (2020).
[33] R. Tat, Semiclassical Floquet-Markov master equation for Monte Carlo spin integration, Phys. Rev. A **112**, 013113 (2025).
[34] *Heun's Differential Equations*, edited by A. Ronveaux (Oxford University Press, New York, 1995).
[35] S. Y. Slavyanov and W. Lay, *Special Functions: A Unified Theory Based on Singularities* (Oxford University Press, New York, 2000).
[36] A. M. Ishkhanyan, T. A. Shahverdyan, and T. A. Ishkhanyan, Thirty five classes of solutions of the quantum time-dependent two-state problem in terms of the general Heun functions, Eur. Phys. J. D **69**, 10 (2015).
[37] A. Khare and B. Mandal, A PT-invariant potential with complex QES eigenvalues, Phys. Lett. A **272**, 53 (2000).